energies

MDPI

Article

Unsteady Flow Field Characterization of Effusion Cooling Systems with Swirling Main Flow: Comparison Between Cylindrical and Shaped Holes

Tommaso Lenzi *, Alessio Picchi, Tommaso Bacci, Antonio Andreini and Bruno Facchini

DIEF-Department of Industrial Engineering of Florence, University of Florence, via S. Marta 3, 50139 Florence, Italy; alessio.picchi@unifi.it (A.P.); tommaso.bacci@unifi.it (T.B.); antonio.andreini@unifi.it (A.A.); bruno.facchini@unifi.it (B.F.)

* Correspondence: tommaso.lenzi@unifi.it; Tel.: +39-055-2758453

Received: 25 August 2020; Accepted: 16 September 2020; Published: 23 September 2020

Abstract: The presence of injectors with strongly swirled flows, used to promote flame stability in the combustion chambers of gas turbines, influences the behaviour of the effusion cooling jets and consequently of the liner's cooling capabilities. For this reason, unsteady behaviour of the jets in the presence of swirling flow requires a characterization by means of experimental flow field analyses. The experimental setup of this work consists of a non-reactive single-sector linear combustor test rig, scaled up with respect to the real engine geometry to increase spatial resolution and to reduce the frequencies of the unsteadiness. It is equipped with a radial swirler and multi-perforated effusion plates to simulate the liner cooling system. Two effusion plates were tested and compared: with cylindrical and with laid-back fan-shaped 7-7-7 holes in staggered arrangement. Time resolved Particle Image Velocimetry has been carried out: the unsteady characteristics of the jets, promoted by the intermittent interactions with the turbulent mainstream, have been investigated as their vortex structures and turbulent decay. The results demonstrate how an unsteady analysis is necessary to provide a complete characterization of the coolant behaviour and of its turbulent mixing with mainflow, which affect, in turn, the film cooling capability and liner's lifetime.

Keywords: film cooling; gas turbine; swirling flow

1. Introduction

In modern gas turbine combustors, highly swirling flow structures are used to promote the fuel-air mixing and to provide stable flames. Due to the complex flow field generated by these type of injectors and to their interactions with liner walls make the correct estimation of heat load an hard task. As a direct consequence of this, understanding the effects of the swirling flow on near-wall flow field is fundamental in order to support the development better effective cooling schemes and improve combustors durability. One of the most promising cooling technology for liners is the so-called effusion technique that allows high cooling effectiveness, due to both the formation of a cold air layer between walls and hot gases and the production of a strong heat sink effect. In the open literatures several authors have proposed different cooling hole geometries aimed at increasing their effectiveness; among these the laid-back fan-shaped fully expanded holes [1] are frequently used for their relative easy manufacturability, by laser drilling or EDM.

Fundamental experimental studies on cylindrical and shaped holes were proposed by several authors [2–5] with the final aim of measuring flow field with non intrusive laser diagnostics, typically developing test rigs with axial and uniform main flow. More recently, with the aim of reproducing similar conditions to those present in the combustion chambers, several authors proposed

the introduction of a swirling mainstream, to focus their studies on the mutual interactions between the swirling and coolant flows [6,7] on liner time-averaged thermal characteristics.

However, considering the presence of the unsteady structures in the coolant jets [8] and of the swirling flow which affect the turbulence in the proximity of the cooled liner surfaces, time-resolved measurements techniques are fundamental to correctly understand the effusion film mixing and behaviour. For this reason a Time-Resolved PIV campaign has been carried out by Eberly and Thole [9] to characterize cylindrical holes with axial mainstream, by varying the classical fluid-dynamics parameters that influence the jets behaviour (i.e., blowing ratio BR, velocity ratio VR, momentum ratio I) and obtaining results in terms of turbulence and vorticity. Abram et al. [10], Straubald et al. [11] applied thermographic Particle Image Velocimetry, which also gives time resolved temperature data, on a trenched hole geometry, showing that, due to the unsteadiness of the jets, hot gases pass through the coolant sub-layer and frequently reaches the liner surface. These phenomena reveal that the instantaneous gas temperature nearby the liner could be strongly higher than what is suggested from the average temperature field.

The final purpose of this work is to characterize the effusion cooling behaviour in terms of flow field, using Time Resolved PIV technique, under the effect of a representative swirling flow. The analysis of the results focuses on the comparison between cylindrical and shaped holes. The work can be considered the continuation of the work published by the authors regarding the behaviour of standard cylindrical holes [12] in the same environment. The adoption of a swirling main flow allows to complement the analysis of these cooling arrangements generally available in the open literature with an axial uniform main flow, including a comparison between cylindrical and shaped configurations.

In this work a characterization of the main flow pattern is initially presented. Following an in-depth focus to the cooling jets behavior is shown by varying the feeding pressure drop across the multi-perforated plates.

2. Experimental Facility

The test rig (Figure 1), operated in the open loop wind tunnel of the THT LAB at the University of Florence, consists of a non-reactive single sector planar rig working at ambient temperature; it allows the control of two separated flows—the mainflow, which enters into the test section across a swirler, and the cooling flow, to feed an effusion plate. The swirler, specifically designed for aero-engine combustors, is characterized by a marked radial configuration.

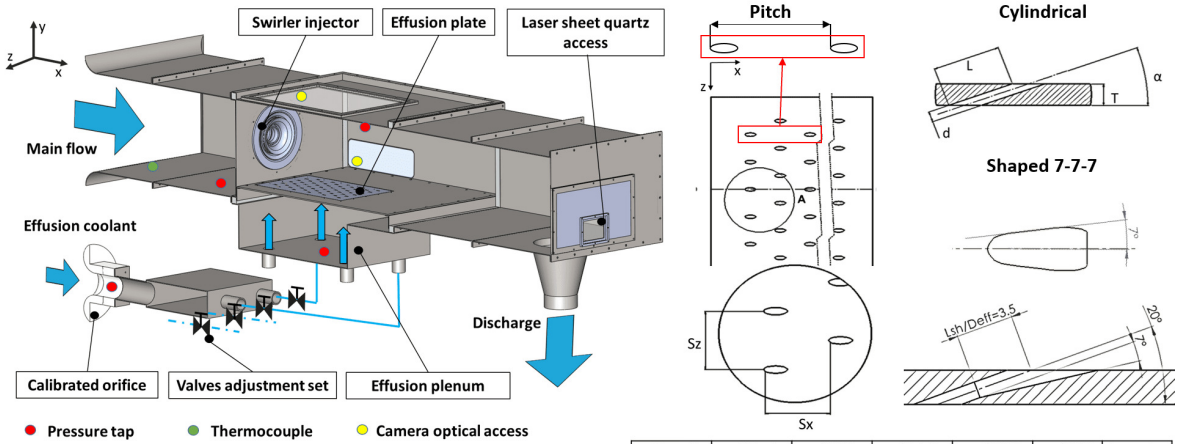

d [mm]	α [deg]	L/d [-]	T/d [-]	Sx/d [-]	Sz/d [-]	Porosity
6.08	20	6	2.1	8	8	5%

Figure 1. Scheme of the test rig and effusion plates geometry.

Downstream of the injector, on the bottom wall of the test section, two different multiperforated plates, with cylindrical and shaped cooling holes respectively, can be installed, to mimic an effusion

cooled liner. A 90 kW centrifugal blower, with a maximum flow rate capability of about 8400 m^3/h, is connected to the discharge duct of the rig. Compared to typical engine dimensions, the rig was scaled up in order to increase the spatial resolution of the measurements, preserving the Reynolds number of the swirling flow. Moreover, a scaled up geometry helps in reducing the characteristic frequency of the unsteady phenomena.

The 55 holes of the effusion plates are in staggered configuration forming 10 cooling rows. As shown in the right part of Figure 1, the holes have an inclination of 20°. The laid-back fan-shaped cooling holes geometry is the so called 7-7-7 developed by Schroeder and Thole [13]. The leading edge of the first horizontal row of holes has a distance of 0.9 and 0.75 swirler external diameters (D_{ref}) respectively from the dome wall and from the swirler prefilmer (where the x = 0 value is located). All the geometrical information concerning the two multiperforated plates are summarized in Figure 1. The rig is equipped with 3 optical accesses to conduct PIV measurements: glass windows are utilized for the laser sheet entrance and for the camera acquisitions on the measurement planes. During the tests a constant pressure drop across the injector (3.5%) was set. Indeed, in order to test different mass flow rates of the coolant system, the test rig is provided with four 2" valves; this feeding system allow a precise regulation of the pressure drop through the effusion plates. The dimensions of the cooling system supply plenum guarantee almost static conditions of plate feeding flow. The pressure drop of the effusion system was regulated from 1% to 3.5% in order to evaluate its impact on the results and extend the applicability of the investigation to different cooling geometries and configurations with lower feeding pressure drop across the effusion plate with respect to the swirler nozzle condition, such as double-wall schemes [14,15]. At the reference operating conditions (feeding pressure drop = 3.5%) the Reynolds number of the main jet is about 515000 while that calculated on the single coolant jet 22900. The Mach number with a 3.5% pressure drop during the test conditions is equal to 0.22. Calibrated orifices were used to measure main and coolant mass flow rates. One of them, as sketched in Figure 1, is positioned upstream of the coolant valves, to directly measure the coolant mass flow, while the second is located downstream of the discharge of the test rig, allowing to measure the sum of mainstream and coolant mass flow rates.

3. Instrumentation and Measurement Technique

All the measures of the flow field presented in this work were made by means of 2D Particle Image Velocimetry technique. The three investigated planes are shown in Figure 2. A Phantom Miro M340 camera and a Nd:YAG pulsed laser (*Litron LDY*303), operating at a wavelength of 527 nm, were used. The synchronization between camera and laser as well as the acquisition and the post process of the images was performed by *DantecDynamicStudio* 4.0 software. Regarding seeding particles, the synthetic oil particles were generated by means of a Laskin nozzle with a Sauter mean diameter of about 1 µm [16] and introduced upstream the swirler and the coolant plenum chamber. The investigation is limited to the bottom half of the test cell, where the effusion cooling plate is positioned. The flow field measurements were carried out on the three spatial planes up to the seventh row of holes. A 60 mm macro lens was used for the xy and xz planes, while a 150 mm one was used for the zy plane; a spatial resolution of about 11.4 and 8 pixel/mm was achieved respectively. The view on the zy plane is downstream to upstream and the results will also be shown in this way. For the steady state analysis of the main flow in the xy plane the whole investigated area was 200 × 500 mm and it was measured with six laser/camera different positions with an acquisition frequency of 0.5 kHz. To combine the different six acquisitions, an overlap of the adjacent FoVs by 25 mm was performed. The velocity measured values were then interpolated in the overlapping areas to merge the obtained results. For the coolant sub-layer analysis the acquisition frequency was increased up to the 3.0 kHz range reducing the camera resolution (image crop). For each Field of View (FoV), 1500 pairs of camera acquisitions were post-processed and average in order to obtain an high statistical convergence. The optical setup for the laser sheet generation consists of 2 planar concave

and one planar convex spherical lenses to adjust the focal line of the laser sheet on the center of each investigated area, and of one or two cylindrical lenses to regulate the laser sheet aperture. The thickness of the laser sheet in the measured planed is between 0.5 and 1.0 mm. An Adaptive cross-correlation method has been used to calculate the velocity fields [17]. During the cross-correlation iterative method the interrogation area (IA) refinement begins from a 64 × 64 pixel first windows to a third final size of 16 × 16 (passing from a 32 × 32 second step) with 50% overlap between two consecutive interrogation areas. The universal outlier detection method [18] was used for the vector validation and the outliers were substituted by linear interpolation of the neighbour vectors. The uncertainties on the velocity measurements is within 4%, calculated using the method described by Charonko and Vlachos [19] that consists in correlating the uncertainty bounds to the first and second cross-correlation peaks ratio.

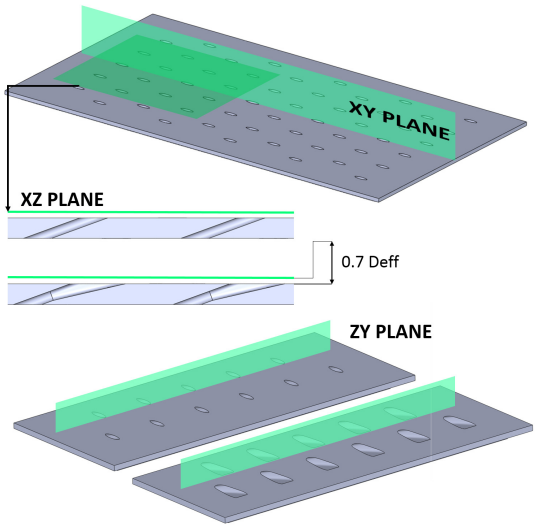

Figure 2. PIV measurement planes.

4. Main Flow Results

4.1. Swirling Flow Characterization

This section shows a characterization of the main flow field to better estimate its impact on the steady and unsteady behaviour of the effusion jets. The flow field promoted by the swirler is reported in Figure 3. The measurements were reported at reference condition in terms of swirler and effusion pressure drop ($\Delta P/P = 3.5\%$) focusing on the case with the cylindrical effusion plate. The image in the top refers to the flow field on the meridian plane (xy) while the bottom one to the plane parallel to the dome (zy). The zy plane, that is placed at the leading edge of the first row of holes, give information of the flow field immediately upstream of the coolant injection. V_{PIV} is used to show the magnitude of the 2D velocity on the analyzed measurement planes. Indeed the normal component of the velocity cannot be estimated with the presented measurement setup. A reference value V_{ref} is used to normalized the V_{PIV} velocity.

Focusing the attention on the xy plane, all the classical features of a swirling flow field are recognized with a common shape of the swirler jet, characterized by high velocity and the formation of inner and outer shear layers. The wide opening angle of the main jet promote the impinging of the swirling flow on the effusion plate near the dome, before the first row of holes at around $x/D_{ref} = 0.3$. Downstream the stagnation region the flow field is characterized by an acceleration that produces a strong interaction, between the main flow and the coolant flow field, measured up to the third row of holes. A vortex breakdown occurs in the test section with a large central recirculation. Under the swirling jet a very confined small corner vortex region is recognizable. Additional details of the mainflow investigation on the xy plane can be found in the previous work [12], where different results had already been shown.

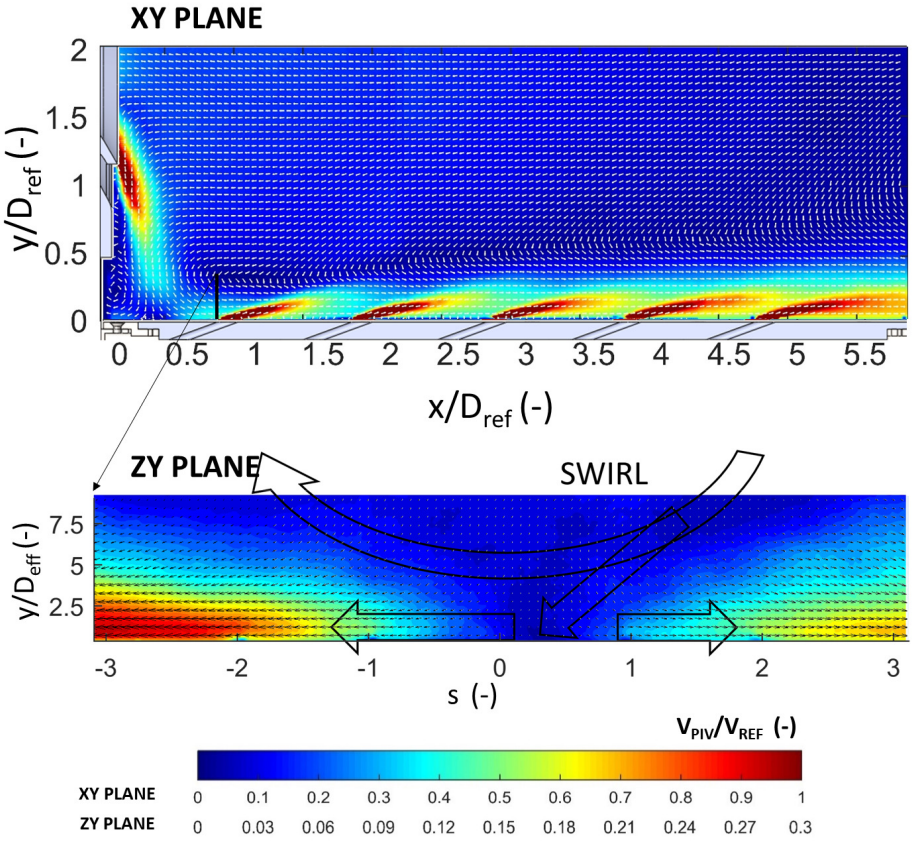

Figure 3. Mean flow field on XY and ZY planes.

Concerning the zy plane, in which the rotating flow field is clearly visible, it is possible to notice how the swirling flow creates a stagnation point just on the right side respect to the center point located in $s = 0$ according to the direction of rotation of the flow. This interaction with the liner wall promotes two high-velocity areas moving away from the stagnation point, with the higher velocity values located on the left hand side. As a consequence, this strong flow field asymmetry affects the effusion jets behavior.

To conclude the characterization of the main flow, providing information about its unsteady behaviour, Figure 4 shows RMS profiles of the velocity values measured on the xy plane. The five profiles are extracted at different axial position in the region where the main flow develops upstream the first injection. It is possible to notice, for all the profiles, a peak of RMS corresponding to the core of the main jet. The trend shows a reduction of the peak intensity moving towards the first hole (i.e., increasing x/D_{ref}). Nevertheless, the profile close to the first hole (black line), still shows a RMS peak approaching the effusion jets. As a general observation it can be expected that, starting from the first row of holes, the effusion cooling jets are affected by a main flow characterized by high RMS values generated by the strongly unsteady nature of the swirling flow. Additional information about the energy and frequency content of the main flow unsteadiness near the wall are provided in previous work on this test rig [12]. The previous PIV and hot wire anemometry analyses highlighted time-coherent flow structures associated to the precessing vortex core (PVC) at the output of the injector. However, near the liner, the spectra of kinetic energy showed a flattening of the spectrum. So the behavior of the coolant is not influenced by the pulsating effect of PVC. However was highlighted an intense interactions, of intermittent nature without a specific frequency, between the swirling flow and the effusion plate.

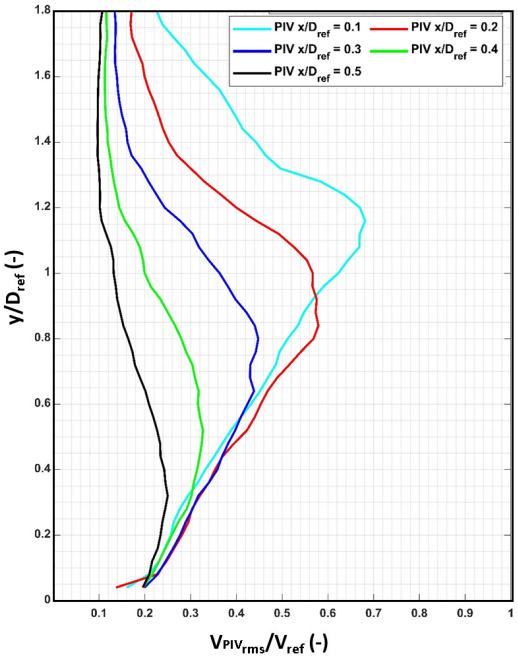

Figure 4. Root Mean Square (RMS) of velocity profiles measured downstream the swirler.

5. Effusion Flow Results

5.1. Average Flow Field Analysis

Figure 5 shows velocity contours for the xy and zy planes changing the cooling pattern: cylindrical on the left and shaped holes on the right. Focusing the attention to the xy plane for both the tested geometries, due to the low inclination of the injection angle, the cooling jets create an effective coolant sub-layer. Moreover the consecutive jets injection promotes a clear film superposition with a coolant substrate characterized by high velocity values. From the comparison it is visible how, for the shaped holes, a more defined and confined coolant sub layer is achieved, with respect to the cylindrical ones. It is characterized by homogeneous velocities and reduced thickness thanks to the effect of the laid-back angle. On the other hand, for the cylindrical case despite the low value of injection angle, it is possible to detect defined structures of the jets with higher penetration capacity and jet velocity. Thanks to the wide discharge area, the shaped configuration presents lower and more homogeneous velocity distribution with a strong reduction of velocity peaks.

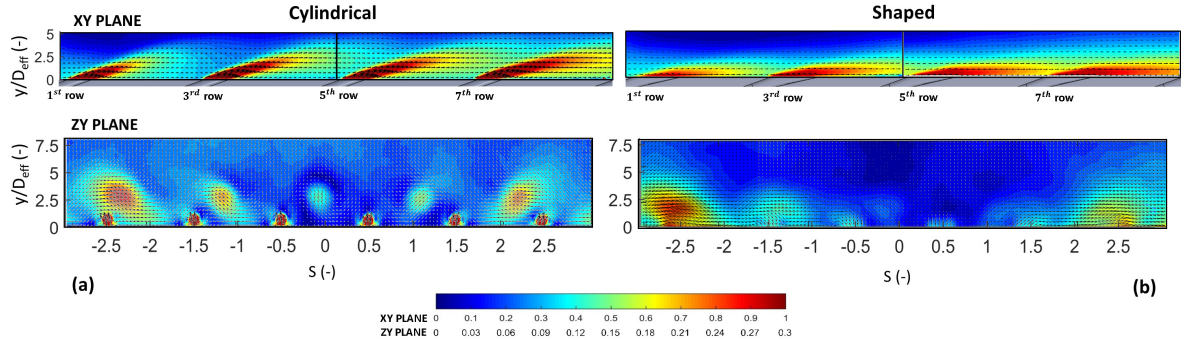

Figure 5. Effusion flow field plane for cylindrical (**a**) and shaped (**b**) geometry.

The interaction between swirling and coolant flow, for both geometries, has a different behaviour from what is usually reported in presence of uniform main flow [4], where the consecutive jets are usually closer to the liner wall due to the effect of the superposition of the coolant. In the present test

case the swirling flow tends to crash the first cooling jet toward the liner while the trajectories of the following rows progressively move away from the wall. The bottom part of Figure 5 shows the velocity values on the zy plane at the trailing edge of the second row of holes. Also in this case it is possible to see the higher velocities of the cylindrical holes immediately exiting from the holes which generate a flow field with well defined circular spots (jets core). The shaped hole, thanks to the higher exiting area, present lower velocity values and a more homogeneous and spread flow field that helps to cover more effectively the liner wall. A strong effect of the main flow on the trajectory of the jets can be noted as well. For both geometries the core of the jets of the previous row is still detectable at the trailing edge of the second row; again, higher velocity in coherent structures can be appreciated for the cylindrical holes, while the shaped configuration results in lower velocity within less defined flow structures, closer to the liner wall. Observing the residual velocity spots of the first row, there is a shift of the jets core according to the asymmetric main flow field and velocity spots shown in Figure 3. The lateral shift of the jet traces prompted by the swirl flow could have a strong impact on the film capability since an interaction between consecutive jets is clearly visible in the flow field, reducing the beneficial effect that the staggered configuration should be supposed to provide. A higher lateral displacement (and therefore row-to-row interaction) can be appreciated for the shaped holes, due to the lower momentum of the coolant jets. Even if it is not reported in the results, this overlapping phenomena of the jets was found on all the measured row for both geometries (up to the fourth) with a progressive weakening of the phenomenon moving away from the swirler. Finally, looking to the lateral spots of the jets from the previous row ($s = \pm 2.5$), it is clear how the cores of the jets assume a stretched and elongated shape, far from the classical behaviour in the presence of an axial flow [20–22]. It is possible to speculate that such a strong deviation underline that any correlative approach to estimate cooling effectiveness based on formulations developed on fundamental test cases could be completely ineffective especially in the near dome region.

5.2. Jets Oscillations

To better understand the dynamics of main-coolant interaction, the top part of Figure 6 presents a temporal evolution of the unsteady structures of the swirling flow that interact with the first effusion row (feeding pressure drop—$\Delta P/P = 3.5\%$, cylindrical plate). Looking at the first snapshot ($t = 0$ s) it is possible to see the presence of a structure from the swirler, highlighted in red on the top left side of the figure, that is approaching the jet of the central hole of the first row. At $t = 0.0013$ s and $t = 0.0026$ s, the main flow turbulence spot crushes the cooling jet to the liner wall and the second part of jet is dragged away from the jet of the main flow. The fourth snapshot ($t = 0.0040$ s) show a cooling jet still well structured and defined but completely attached in its length to the plate. Continuing the analysis with the following snapshots, thanks the absence of further structures from the main flow, the jet restabilizes with a trajectory in line with the inclination of the hole. This dynamic occurs whenever turbulent spots of the main flow interact with the jets. Reducing the plate feeding pressure drop, the oscillatory phenomena and the crushing of the jets to the wall increase due to the reduction of the jet momentum. However, significant changes in trajectory were detected only up to the fourth row of holes. For a better quantitative analysis of the oscillations, by varying the feeding pressure drop and the distance from the swirler, the central part of Figure 6 shows instantaneous streamlines for cylindrical (left) and shaped (right) geometries. For the calculation of the streamlines the approach proposed by Reference [23] has been used. For each image the streamlines are calculated starting from the center of the holes using the "streamline" Matlab function: every streamline therefore visualizes the flow condition of one single snapshot which however well represent the fluctuation of the cooling jet trajectory. The streamline plots in Figure 6 concern the first and third rows on the meridian plane. In each plot 100 streamlines are drawn using red lines for $\Delta P/P = 3.5\%$ and black lines for the 1% case. The results underline an extremely different behaviour between the two geometries. For the shaped holes, even near the swirler (first row), a highly stable jets evolution occurs as evidenced by the reduced spreading of the streamlines varying the feeding pressure drop. For both $\Delta P/P = 1\%$ and 3.5% the jet

of the first and third row is constantly attached to the wall. On the other hand, the cylindrical geometry suffers more the influence of the main stream flow. With a $\Delta P/P = 1\%$ the behaviour is completely unstable up to the third row, with the instantaneous streamlines which present a spread and chaotic distribution. Only with a $\Delta P/P = 3.5\%$ and from the third row the jet has less spread streamlines and quite a stable evolution. This type of analysis is summarized, taking into account the entire statistical sample (1500 instantaneous snapshots for case), in the probability density functions (PDF) reported on the bottom part of the same Figure 6. The histograms are made tracking the y position of the velocity maximum values measured at 50% of the row-to-row pitch for each snapshot (see Figure 1 for the pitch definition). For the first cylindrical row there is a continuous ($\Delta P/P = 1\%$) and a significant ($\Delta P/P = 3.5\%$) interaction with the wall due to the intermittently squashing of the jet as previously shown. Different behaviour is registered for the third row. PDF assumes a Gaussian trend with high values of standard deviation and jet wall interaction for $\Delta P/P = 1\%$. Increasing the feeding pressure drop ($\Delta P/P = 3.5\%$) the jet appear stable and constantly detached from the wall. As far as the shaped geometry is concerned, jets show a more stable behaviour for all the investigated cases, since the coolant flow is more attached to the wall and less sensitive to the mainstream induced fluctuations.

It can be concluded that for what concern the jets oscillations on the xy plane the cylindrical holes are clearly more prone to jet oscillation and the strong penetration promotes a coolant jet washing phenomena described by the flow field snapshots.

5.3. Flow Structures Investigation

5.3.1. Kelvin Helmholtz Instability

A study of the shear layer instabilities which characterize the effusion cooling jets were made on the meridian plane. In the results the 2D vorticity values w were scaled by the exit jet velocity $V_{3.5\%}$, measured at the reference condition $\Delta P/P = 3.5\%$, and D_{eff}. In the left side of Figure 7, for both geometries the K-H anti-clockwise (red) and the K-H clockwise vortices (blue) are plotted with a zoomed view on the hole exit region for $t = 0$ s. These unsteady structures are the product of the interaction between the shear layer of the jet and the surrounding flow. The K-H clockwise vortices are produced on the hole trailing edge and are positioned on the bottom part of the shear layer of the jets; the anticlockwise vortices, on the other hand, are located on the upper shear layer and evolve from the leading upstream edge of the film cooling hole. Figure 7 (left) reports the time evolution of K-H instabilities for the third row ($\Delta P/P = 3.5\%$). Moving away from the holes these instabilities are convected downstream with the mean flow and the vorticity structures progressively decay to a homogeneous turbulent development. After 60% of the pitch for cylindrical holes and 30% for shaped geometry it is not possible to identify coherent eddies structures. In the cylindrical geometry the instabilities have a coherent and well-defined structure with a defined lengthscale of the eddies of about one hole diameter. A different behaviour is detected for the shaped case. In absolute terms the vorticity values are reduced, the structures have a less coherent shape and a very rapid decay with a not well-defined lengthscale, due to the diffused exit hole.

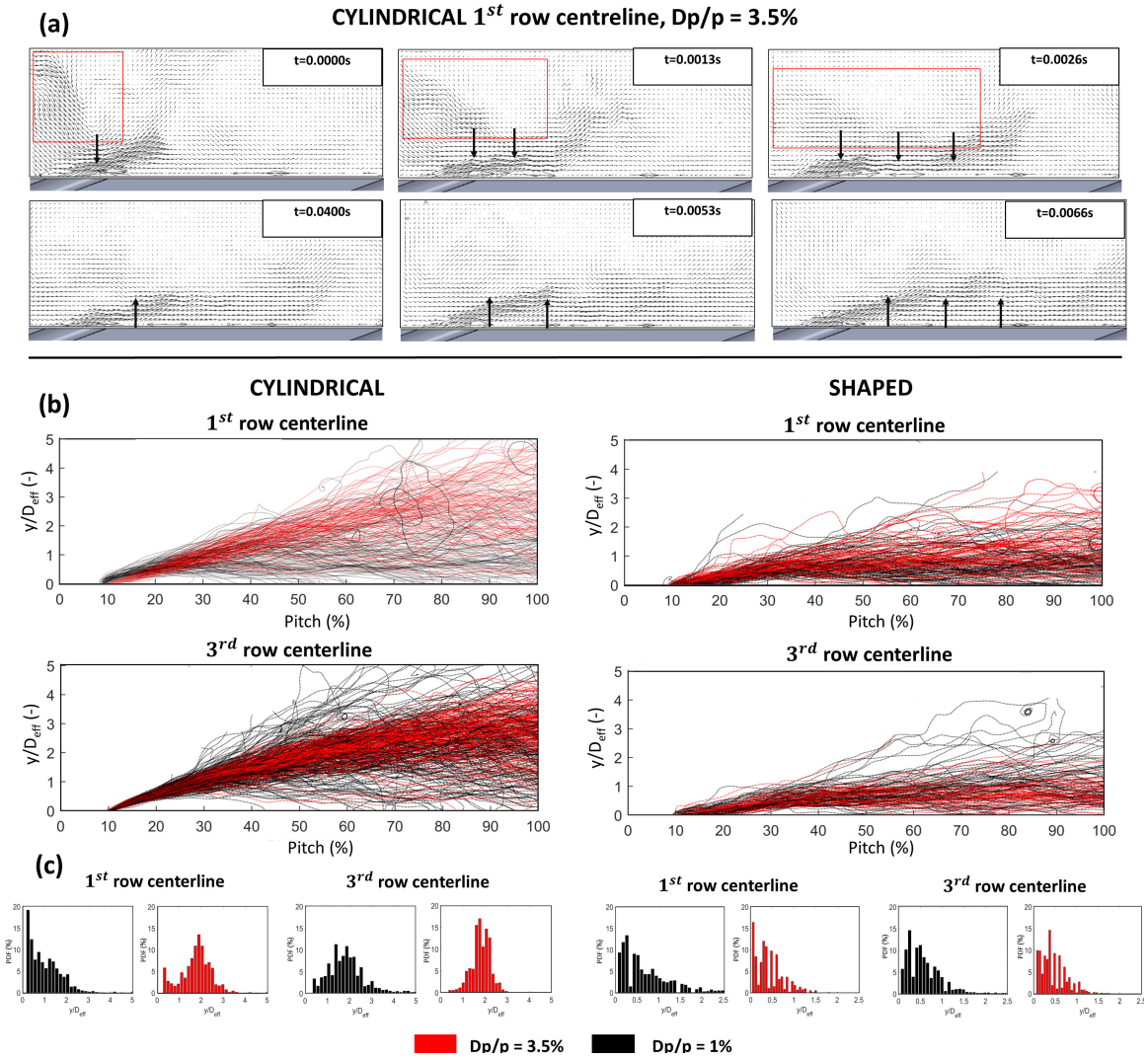

Figure 6. (**a**) First effusion jet and swirling flow unsteadiness interaction. (**b**) Instantaneous velocity streamlines starting from the center of the holes by varying the pressure drop: cylindrical geometry on the left and shaped on the right. (**c**) PDF of the velocity maximum y position for $x = 50\%Pitch$. Black line = $\Delta P/P = 1\%$; red line= $\Delta P/P = 3.5\%$.

To verify the effect of the coolant feeding pressure drop on the vorticity magnitude and its decay process, the right part of Figure 7 also reports the y-averaged vorticity absolute values measured on the jet structures at different x positions. Looking at the profiles of cylindrical geometry it is recognizable how the counterclockwise vortices, originated in the upstream edge of the holes (pitch = 0%), produce a peak of vorticity for all the rows and pressure drops. The following second peak, with an offset equal to the trace of the hole, is connected to the development of the clockwise vortices. This contribution of negative vorticity is lower due to the absence of a direct interaction with the free stream and the continuous interaction with the wall. In fact the swirling flow crushes the jets to the wall impeding the development of vorticity. For shaped geometry a second peak is never manifested. This is in line with the velocity measurements summarized in the probability density functions—the jets produced by the 777 geometry generate a sub-layer constantly attached to the wall preventing from the formation of a bottom shear layer. As a general consideration, the vorticity values of the shaped jets are very low, reflecting a reduced tendency to promote eddy structures. Moving to the description for each jet and taking in account the variation of the feeding pressure drop (Figure 7), for all jets and for both geometries the peak vorticity value reduces with the $\Delta P/P$ due to the decreasing of the velocity ratio. Focusing on the cylindrical geometry at the first hole, for each pressure drop values,

a second peak cannot be observe due to the interaction between the jet and the liner wall as previously explained. The third row of holes, that is also subjected to an intermittent crushing of the jets to the wall, does not show a second peak for $\Delta P/P = 1\%$. The fifth and seventh rows, less subjected to the swirler interactions, always shows a second peak even if the intensity is much reduced for low pressure drops.

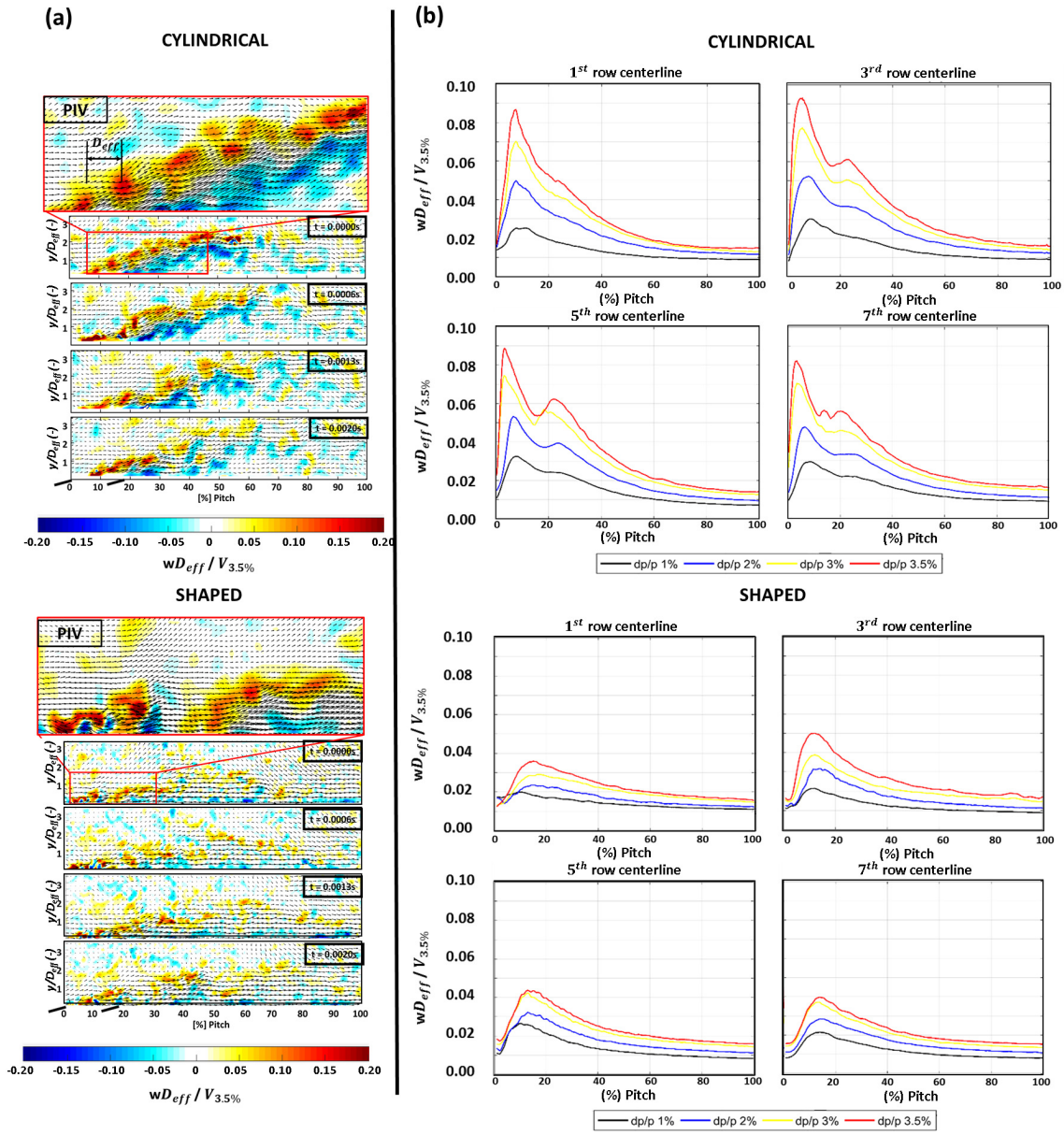

Figure 7. XY PLANE. (**a**) time resolved snapshots of vorticity field ($\Delta P/P = 3.5\%$, third row centerline) for both geometries (top: cylindrical, bottom: shaped). (**b**) Time averaged vorticity profile by varying the feeding pressure drop.

5.3.2. Counter Rotating Vortex Pair

From a steady state point of view the counter rotating vortex pairs (CRVP) are the most important structure that can be observed in the film cooling jets—this secondary flows, like the K-H instabilities, promote entrainment between cooling jet and hot gas with a direct consequence on film effectiveness. The Figure 8 shows, for the second row of holes where the swirling flow effect is still intense, the flow field (superimposed vectors) and the vorticity values acquired on the zy plane.

The classic CRVP structures for the cylindrical case and for the shaped one with smaller values can be recognized; in addition for the 777 geometry, anti-kidney structures are also measured for the central holes and highlighted in the small zoomed view. As a general result it is possible to appreciate the effect of the rotating swirling structure on the jets for both the geometries: a lateral shift of the vortex pairs coming from the upstream row is clearly visible in the cylindrical test case, while for the shaped case this structures are no longer detectable.

Another important observation that introduces an element of novelty with respect to the classical analyses on film cooling holes with axial flow is a sort of torsion of the jets structures in addition to the shift previously highlighted: an anticlockwise torsion on the left side and clockwise on the right side is in agreement with the time average main flow characterization (Figure 3). As a final conclusion it is worth to notice that the shift of the core of the jets generates interactions between the counter rotating vortex pairs of consecutive row of holes: on the left side of the rig ($s = -1.5$), the counterclockwise vortex of first row faced on the clockwise of the second row; an opposite behavior occurs on the right side of the rig ($s = 1.5$).

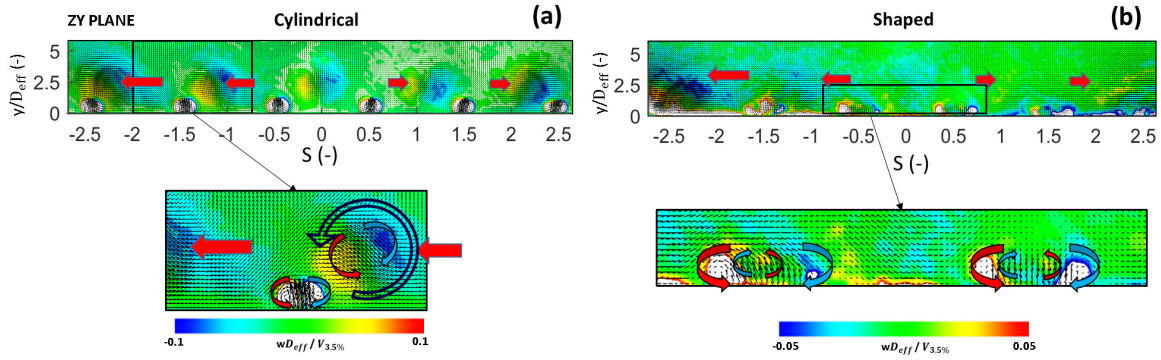

Figure 8. Time average vorticity contours (ZY PLANE) for the second row ($\Delta P/P = 3.5\%$). (**a**) cylindrical and (**b**) shaped geometry.

5.4. Root Mean Square Values

Maps of RMS velocity values on xy, zy, and xz planes are shown in Figure 9 at nominal pressure drop condition ($\Delta P/P = 3.5\%$); all the unsteady phenomena analyses so far are here summarized and quantified. The contribution of Kelvin Helmoltz instabilities is marked with the letter A, B is used for homogeneous turbulence, C for the fluctuations induced by the main flow, E for the wake region, F for the CRVP contribution and G for the mutual interaction between the coolant jets.

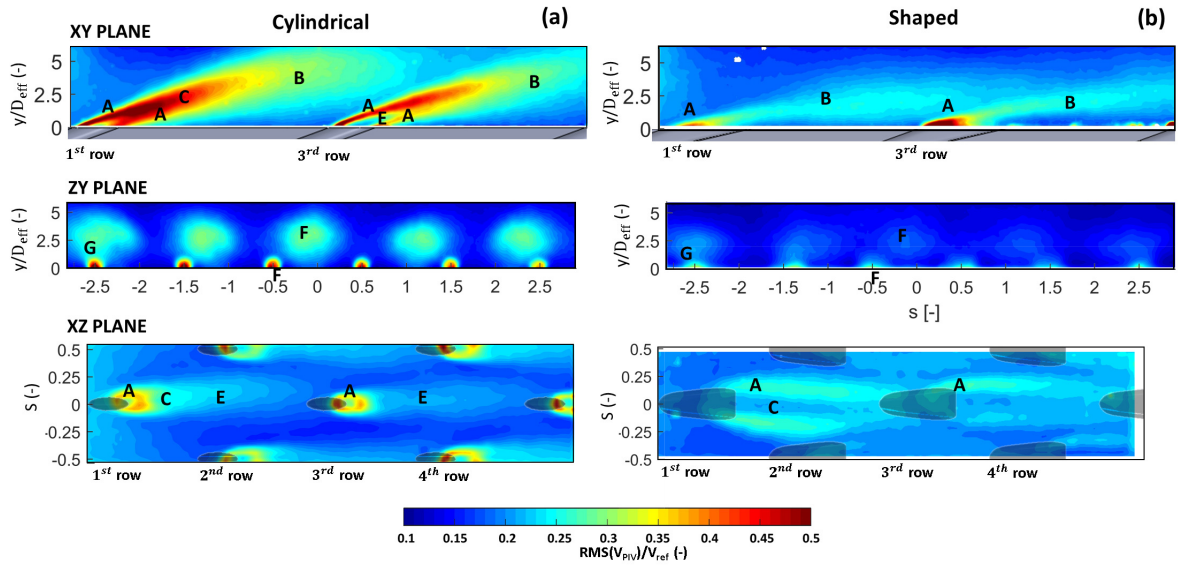

Figure 9. Root Mean Square contours at $\Delta P/P = 3.5\%$ for both geometry ((**a**): cylindrical. (**b**): shaped) for the three spatial planes.

Looking at the first plane (xy) for the cylindrical geometry, in accordance with the vorticity analysis on the meridian plane, strong values of RMS are achieved on the shear layer of the jets (A) starting from both the leading and the trailing edge of the holes where the K-H instabilities are generated and convected downstream.

K-H contributions merge in region (B) due to turbulence decay—in this region the RMS maps appear more homogeneous and the intensity decrease moving away from the holes. For the shaped case, only the upstream shear layer contributes to the velocity fluctuations generated by K-H instabilities in accordance to the vorticity analysis. Moreover, the decay process start close to the hole exit moving to a wide homogeneous turbulence area (B). The contribution of this vortices is also detectable in the xz plane for both geometries (A) as a circular track for the cylindrical case and as two strips for the shaped one.

Another source of flow instability marked with the letter E for the cylindrical case is located where potential reattachment, jet oscillation and wake vortices generate high turbulence levels measured in the xy and xz planes.

For both geometries, as highlighted in xy and xz planes, the central hole of the first row is characterized by higher RMS values (C) with respect to the following rows. This high values can be justified by the intermittent interaction with the main jet, which convects large energy-carrying vortices producing the jets oscillation and crushing.

Finally, looking to zy plane it is also possible to recognize the contribution of unsteady terms of the CRVP (F) and of the mutual interaction between the jets of consecutive rows (G). Also in this plane the RMS values measured for the shaped geometry are very small compared to the cylindrical one.

6. Conclusions and Perspectives for Future Work

A PIV campaign was carried out on a non-reactive single sector combustor simulator rig working in ambient conditions; it was equipped with two effusion cooled plates provided with cylindrical and laid-back fan-shaped holes (777) respectively. The purpose of this work was to characterize the behaviour of these two different geometries under the effect of a representative swirling main flow. Different pressure drops across the cooled plate are imposed to also estimate the impact of the velocity ratio on the interaction between the main and coolant flow.

The analysis showed jets behaviour which is strongly affected by the swirling flow, resulting in:

- deviation of the jets trajectories,

- mutual interaction between jets of consecutive rows despite the staggered configuration,
- shift and torsion of CRVP structures
- jet oscillations and intermittent interaction with the main flow

Finally, the analysis allows to directly compare the behaviour of cylindrical and shaped holes. Despite the shaped geometry exhibited a slight increase in the lateral shift prompted by the rotating structures of the swirler, it seems less affected by oscillatory phenomena and jet crushing on the xy plane. In addition, lower RMS velocity values were registered on all the investigated plane with a quick axial vorticity decay.

The following activities of the shown research work will be focused on quantifying the differences highlighted between the two geometries in terms of thermal performance.

Author Contributions: T.L., A.P. and A.A. conceived and designed the experiments. T.L., A.P. and T.B. carried out the experiments and analyzed the data. T.L. wrote the paper. B.F. supervised the whole process and checked the paper. All authors have read and agreed to the published version of the manuscript.

Funding: This research was funded by European Union's Horizon 2020 research and innovation programme under Grant Agreement No. 690724.

Acknowledgments: The authors wish to gratefully acknowledge SOPRANO (SOot Processes and Radiation in Aeronautical inNOvative combustors) Consortium for the kind permission of publishing the results herein.

Conflicts of Interest: The authors declare no conflict of interest. The funders had no direct role in the collection, analyses, or interpretation of data; in the writing of the manuscript, or in the decision to publish the results.

Abbreviations

The following abbreviations are used in this manuscript:

$\Delta P/P$	Feeding pressure drop	[%]
BR	Blowing Ratio	[−]
D_{eff}	Effusion hole diameter	[m]
D_{ref}	External swirler diameter	[m]
f	frequency	[Hz]
I	Momentum Flux Ratio	[−]
$Pitch$	Axial pitch of effusion pattern	[m]
$\%Pitch$	Percentual value of the Pitch distance	[%]
s	Scaled lateral pitch of effusion pattern	[−]
RMS	Root Mean Square	[m/s]
t	time	[s]
w	Vorticity	[1/s]
V	Velocity magnitude	[m/s]
VR	Velocity Ratio	[−]
x, y, z	3D Spatial coordinates	[m]
3.5%	3.5% nominal pressure drop	
41	Referred to Plane 41	
eff	effusion system	
PIV	PIV measurements	
ref	Reference value	
FoV	Field of View	
PIV	Particle Image Velocimetry	
RQL	Rich-Quench-Lean	
TRPIV	Time-Resolved Particle Image Velocimetry	

References

1. Colban, W.; Thole, K.A.; Haendler, M. A comparison of cylindrical and fan-shaped film-cooling holes on a vane endwall at low and high freestream turbulence levels. *J. Turbomach.* **2008**, *130*. [CrossRef]
2. Gustafsson, K.M.B. *Experimental Studies of Effusion Cooling*; Chalmers University of technology, Department of Thermo and Fluid Dynamics: Gothenburg, Sweden, 2001.
3. Thole, K.; Gritsch, M.; Schulz, A.; Wittig, S. Flowfield Measurements for Film-Cooling Holes With Expanded Exits. *ASME J. Turbomach.* **1998**, *120*, 327–336. [CrossRef]
4. Scrittore, J.J.; Thole, K.A.; Burd, S.W. Investigation of Velocity Profiles for Effusion Cooling of a Combustor Liner. *ASME J. Turbomach.* **2006**, *129*, 518–526. [CrossRef]
5. Fernandes, P.; Hodges, J.; Fernandez, E.; Kapat, J.S. Flow Statistics and Visualization of Multi-Row Film Cooling Boundary Layers Emanating From Cylindrical and Diffuser Shaped Holes. *J. Turbomach.* **2018**, *14*, 06105. [CrossRef]
6. Wurm, B.; Schulz, A.; Bauer, H.; Gerendas, M. Impact of Swirl Flow on the Cooling Performance of an Effusion Cooled Combustor Liner. *ASME J. Eng. Gas. Turb. Power* **2012**, *134*, 121503. [CrossRef]
7. Andreini, A.; Becchi, R.; Facchini, B.; Mazzei, L.; Picchi, A.; Turrini, F. Adiabatic Effectiveness and Flow Field Measurements in a Realistic Effusion Cooled Lean Burn Combustor. *ASME J. Eng. Gas. Turb. Power* **2015**, *138*, 031506–031506–11. [CrossRef]
8. Fric, T.F.; Roshko, A. Vortical Structure in the Wake of a Transverse Jet. *J. Fluid Mech.* **1994**, *279*, 1–47. [CrossRef]
9. Eberly, M.K.; Thole, K.A. Time-Resolved Film-Cooling Flows at High and Low Density Ratios. *ASME J. Turbomach.* **2013**, *136*, 061003. [CrossRef]
10. Abram, C.; Schreivogel, P.; Fond, B.; Straubald, M.; Pfitzner, M.; Beyrau, F. Investigation of Film Cooling Flows using Thermographic Particle Image Velocimetry at a 6 kHz Repetition Rate. In Proceedings of the 18th International Symposium on the application of Laser and Imaging Techniques to Fluid Mechanics, Lisabon, Portugal, 4–7 July 2016.
11. Straubald, M.; Schmid, K.; Hagen, M.; Pfitzner, M. Experimental and Numerical Investigation of Turbulent Mixing in Film Cooling Applications. In Proceedings of the Turbo Expo: Power for Land, Sea, and Air. American Society of Mechanical Engineers, Charlotte, NC, USA, 26–30 June 2017.
12. Lenzi, T.; Palanti, L.; Picchi, A.; Bacci, T.; Mazzei, L.; Andreini, A.; Facchini, B. Time-Resolved Flow Field Analysis of Effusion Cooling System With Representative Swirling Main Flow. *J. Turbomach.* **2020**, *142*, 061008. [CrossRef]
13. Schroeder, R.; Thole, K. Adiabatic Effectiveness Measurements for a Baseline Shaped Film Cooling Hole. In Proceedings of the Turbo Expo: Power for Land, Sea, and Air. American Society of Mechanical Engineers, Düsseldorf, Germany, 16–20 June 2014.
14. Andreini, A.; Cocchi, L.; Facchini, B.; Mazzei, L.; Picchi, A. Experimental and numerical investigation on the role of holes arrangement on the heat transfer in impingement/effusion cooling schemes. *Int. J. Heat Mass Transf.* **2018**, *127*, 645–659. [CrossRef]
15. Nathan, R.; Zhong, R.; Buzzard, W.; Sweeney, B.; Tinker, N.; Ligrani, P.; Hollingsworth, K.; Liberatore, F.; Patel, R.; Ho, S.; et al. Effects of Double Wall Cooling Configuration and Conditions on Performance of Full-Coverage Effusion Cooling. *ASME J. Turbomach.* **2017**, *139*, 051009.
16. Kahler, C.; Sammler, B.; Kompenhas, J. Generation and control of tracer particles for optical flow investigations in air. *Exp. Fluids* **2002**, *33*, 736–742. [CrossRef]
17. Raffel, M.; Willert, C.E.; Kompenhans, J. *Particle Image Velocimetry—A Pratical Guide*; Springer: New York, NY, USA, 1997.
18. Westerweel., J.; Scarano, F. Universal outlier detection for PIV data. *Exp. Fluids* **2005**, *39*, 1096–1100. [CrossRef]
19. Charonko, J.; Vlachos, P. Estimation of uncertainty bounds for individual particle image velocimetry measurements from cross-correlation peak ratio. *Meas. Sci. Technol.* **2013**, *24*, 065301. [CrossRef]
20. Azzi, A.; Jubran, B.; Theodoridis. Film Cooling Predictions of Simple and Compound Angle Injection from One and Two Staggered Rows. *Numer. Heat Transf. Appl.* **2001**, *40*, 273–294. [CrossRef]

21. Kampe, T.; Völker, S.; Sämel, T.; Heneka, C.; Ladisch, H.; Schulz, A.; Bauer, H. Experimental and Numerical Investigation of Flow Field and Downstream Surface Temperatures of Cylindrical and Diffuser Shaped Film Cooling Holes. In Proceedings of the Turbo Expo: Power for Land, Sea, and Air, Orlando, FL, USA, 6–10 June 2011.
22. Schroeder, R.; Thole, K. Thermal Field Measurements for a Shaped Hole at Low and High Freestream Turbulence Intensity. *J. Turbomach.* **2016**, *139*, 021012. [CrossRef]
23. Straußwald, M.; Sander, T.; Bakhtiari, A.; Pfitzner, M. High-Speed Velocity Measurements of Film Cooling Applications at High-Turbulence Main Flow Conditions. In Proceedings of the Turbo Expo: Power for Land, Sea, and Air. American Society of Mechanical Engineers, Oslo, Norway, 11–15 June 2018.